PAPER

Large-area 2D microgel colloidal crystals fabricated via benzophenone-based photochemical reaction†

Junying Weng,[a] Xiaoyun Li,[a] Ying Guan,*[a] X. X. Zhu[b] and Yongjun Zhang*[a]

We report a simple method to fabricate high quality, large area 2D colloidal crystals (CCs) of a soft colloid, poly(*N*-isopropylacrylamide) (PNIPAM) microgel. The microgel spheres were first assembled into a 3D CC. The first 111 plane of the 3D CC close to the substrate was then fixed *in situ* onto the substrate *via* a photochemical reaction of the benzophenone moieties immobilized on the substrate surface. The resulting 2D microgel arrays exhibit a high degree of ordering. The interparticle distance in the 2D array can be tuned by the concentration of the microgel dispersion. Increasing the concentration of the microgel dispersion will reduce the interparticle distance of the resulting 2D array. Because large area 3D microgel CCs can be facilely fabricated, this method allows for the fabrication of large area 2D microgel CCs. In addition, the method allows the 2D CCs to be fabricated on nonplanar substrates.

Introduction

Monodisperse colloidal particles can be assembled into 3D colloidal crystals (CCs) and also 2D CCs.[1–3] Like 3D CCs,[4] 2D CCs have also found important applications, including as photonic crystals,[2] in surface patterns,[5] sensors,[6–9] and nano-lithography.[10,11] Therefore numerous 2D CCs have been prepared by different methods, for example, spin-coating,[12–14] interfacial assembly,[6,7] and convective assembly.[1,15,16] These CCs are usually assembled from hard colloids, such as polystyrene (PS),[6,8,9,16–20] poly(methyl methacrylate) (PMMA),[21,22] and SiO₂.[13,16,23] For example, Kraus *et al.*[16] assembled PS spheres into 2D CCs *via* convective assembly and carefully studied the crystallization mechanisms. Jiang *et al.*[13,23] fabricated non-close-packed 2D CC of silica particles *via* a spin-coating procedure. Recently Meng *et al.*[22] reported the preparation of 2D CC of PMMA colloids by assembling the colloids on an air–water surface.

In contrast, studies on 2D CCs of soft hydrogel colloids, for example poly(*N*-isopropylacrylamide) (PNIPAM) microgel spheres, is relatively sparse.[24] Like hard colloids, monodisperse PNIPAM microgel spheres can be facilely synthesized *via* precipitation polymerization.[25–27] Different from hard spheres, however, PNIPAM microgel spheres could respond to external

stimuli and thus change their size and properties.[26,27] The stimuli-responsivity makes 2D microgel CCs promising for many potential applications. For example, it was found that the attachment and growth of cells seeded on 2D microgel CC can be controlled by temperature.[24] Previously 2D microgel CCs were fabricated *via* dip coating,[28,29] solvent evaporation,[27,30–33] or interfacial assembly.[11,34,35] It was revealed that these soft colloids are more difficult to be assembled into ordered 2D arrays than hard particles, because the 2D ordering is easy to be lost upon drying or transferring, due to the soft nature of the spheres.[24]

Like 2D CCs of hard colloids, there are still some severe limitations for the existing 2D microgel CCs. One problem is that their size is usually small.[6] For example, 2D microgel CCs were previously fabricated by air-drying a diluted microgel dispersion.[30] Although the method is extremely simple, the resulting colored array has a small size of only 0.36 cm² and the ordering is relatively low. Another problem is that most of the methods, for example the spin coating method,[11] only allow for the use of planar substrates. Some methods, for example the one developed by Isa *et al.*[34] requires certain specific equipment (Langmuir trough). To overcome these limitations, we proposed a facile method to fabricate 2D CC of microgel spheres (Scheme 1). The microgel spheres were first assembled into 3D CCs. Then the first 111 plane was fixed *in situ* onto the substrate *via* a photochemical reaction. Because large area, high quality 3D microgel CCs can be facilely fabricated,[36,37] this method allows for fabricating large area, high quality 2D microgel CCs. In addition, non-planar substrates can also be used. We previously used thiol–ene reaction for the fixation purpose.[38] This reaction requires not only the modification of the substrate, but also the microgel spheres. Here a benzophenone-based photochemical reaction was selected to fix the microgel spheres on the

[a]*Key Laboratory of Functional Polymer Materials, State Key Laboratory of Medicinal Chemical Biology, The Co-Innovation Center of Chemistry and Chemical Engineering of Tianjin, Institute of Polymer Chemistry, College of Chemistry, Nankai University, Tianjin 300071, China. E-mail: yingguan@nankai.edu.cn; yongjunzhang@nankai.edu.cn*

[b]*Department of Chemistry, Université de Montréal, C. P. 6128, Succursale Centre-ville, Montreal, QC, H3C 3J7, Canada*
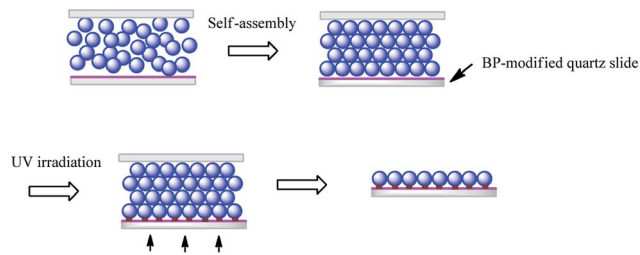
Scheme 1 Fabrication of 2D microgel CC by first assembly of 3D microgel CC followed by *in situ* fixing of the first 111 plane onto the substrate *via* a BP-based photochemical reaction.

substrate.[39–41] In this method the modification of the microgel is no longer required, allowing large area 2D CCs to be fabricated from the pristine microgel spheres.

Experimental

Materials

N-Isopropylacrylamide (NIPAM) and *N*,*N*′-methylenebis(acrylamide) (BIS) were purchased from Alfa Aesar. Acrylic acid (AA) and 3-aminopropyltriethoxysilane (APTES) were purchased from Acros. 4-Aminobenzophenone (ABP), hexahydrophthalic anhydride, *N*-(3-dimethylaminopropyl)-*N*-ethyl-carbodiimide hydrochloride (EDC), potassium persulfate (KPS), *N*-hydroxysuccinimide (NHS) were purchased from local providers. NIPAM was purified by recrystallization from hexane/acetone mixture and dried in a vacuum. AA was distilled under reduced pressure.

Microgel synthesis

A series of PNIPAM microgels with different sizes were synthesized *via* free-radical precipitation polymerization. The 880 nm microgel (hydrodynamic diameter (D_h) = 880 nm at 20 °C) was synthesized as follows. First NIPAM, BIS, and AA were dissolved in 95 mL of water. The total amount of the monomers was 0.015 mol, and their molar ratio, NIPAM : AA : BIS, was 88.5 : 10 : 1.5. The solution was purged with nitrogen and heated to 70 °C. After 1 h, 5 mL of 0.06 M KPS solution was added to initiate the polymerization. The reaction was allowed to process for 4 h. The resulting microgels were purified by three successive centrifugation (12 000g for 1 h) followed by decantation and redispersion in water. To synthesize microgels with bigger sizes, when the above reaction proceeded for 4 h, a 100 mL of pre-heated shell solution was added. The recipes of the shell solution were shown in Table 1. The reaction was allowed to proceed

for additional 4 h. The microgels were again purified by centrifugation followed by decantation and redispersion in water. The microgels were named according to their D_h at 20 °C.

Synthesis of silane coupling agent with a carboxylic acid end functional group[42,43]

Hexahydrophthalic anhydride (326 mg, 1 mmol) was dissolved in 20 mL of anhydrous toluene, to which 23 mL of APTES (1.1 equiv.) was added dropwise. The mixture was stirred at room temperature for 2 h. The solid product was filtered, and recrystallized from petroleum ether/toluene mixture. Yield: 80%. ^{1}H NMR (D$_2$O): δ 0.6–0.78 (t, 2H), 1.16–1.32 (t, 9H), 1.41–1.68 (m, 6H), 1.73–1.85 (m, 2H), 1.87–2.08 (m, 2H), 2.77–2.85 (t, 1H, J = 3.1 Hz), 2.87–2.95 (t, 1H, J = 2.0 Hz), 3.15–3.3 (m, 2H), 3.6–3.74 (q, 6H).

Surface modification of quartz slides

Quartz slides with size of 25 × 45 × 1 mm, unless otherwise specified, were used as substrate for the fabrication of 2D CC. They were cleaned with freshly prepared piranha solution (3 : 7 v/v H$_2$O$_2$–H$_2$SO$_4$ mixture) (**caution**: this solution is extremely corrosive!) for 6 h, rinsed with deionized water thoroughly, and dried in a stream of nitrogen. To introduce surface carboxylic acid groups, the cleaned substrate were immersed in a 15 mM ethanolic solution of the silane coupling agent synthesized above for 12 h at room temperature, rinsed with ethanol extensively, and dried in a stream of nitrogen. To activate the surface carboxylic acid groups, the substrate was immersed in pH 6 phosphate buffer containing EDC (10 mM) and NHS (5 mM) at 4 °C for 2 h, rinsed extensively in deionized water and dried in a stream of nitrogen.[44] The NHS ester-functionalized substrate was then immersed in 20 mM ABP in DMSO at room temperature for 12 h, washed with DMSO extensively, and dried in a stream of nitrogen.[41]

Determination of surface carboxylic acid groups

The amount of carboxylic acid groups immobilized on the surface of the substrate was determined by a colorimetric method based on Toluidine Blue O staining, assuming the molar ratio between carboxylic acid groups and the adsorbed dye to be unity.[41,45] The substrate was first immersed in a 0.5 mM Toluidine Blue O solution (pH 10) at 30 °C for 6 h, and thoroughly washed with pH 10 NaOH solution to remove any dye nonspecifically adhered to the surface. The substrate was then soaked in a 50% acetic acid solution to desorb the dye molecules from the surface. The amount of the released dye was

Table 1 Recipes of the shell solutions for the synthesis of PNIPAM microgels with bigger sizes

Sample name	Total amount of the monomer (mol)	Molar ratio NIPAM : AA : BIS	KPS (M)	D_h at 20 °C (nm)
1450 nm microgel	0.015	90 : 10 : 0	0.003	1450
1550 nm microgel	0.015	89 : 10 : 1	0.003	1550
1800 nm microgel	0.015	88.5 : 10 : 1.5	0.003	1800

then determined from the optical density (OD) of the solution at 633 nm.

Fabrication of 2D microgel arrays

The microgel dispersions were first concentrated by centrifugation. They were then loaded into a cell composed of two quartz slides (one of them was surface-modified) separated by 2 layers of Parafilm. After one day aging at 20 °C the microgel particles self-assembled gradually into a highly ordered crystalline structure. The crystallized samples were then irradiated with UV light ($\lambda > 340$ nm) for 30 min at an integral light intensity of 100 mW cm^{-2}. Finally the reaction cell was opened and the substrate was rinsed in flowing DI water to remove microgel particles not covalently bonded to the substrate.

Characterization

The size and size distribution of microgel particles were determined by dynamic light scattering with a Brookhaven 90Plus laser particle size analyzer. The measurements were all carried out at a scattering angle of 90°. The sample temperature was controlled with a build-in Peltier temperature controller. UV-vis absorption spectra were measured on a TU 1810PC UV-vis spectrophotometer (Purkinje General, China). ^{1}H NMR spectra were measured on a Varian UNITY-plus 400 NMR spectrometer using D$_2$O as solvent. Atomic force microscopy of the 2D arrays was measured on a CSPM5500 scanning probe microscope in tapping mode (Benyuan, China). The optical images were acquired on a Leica TCS SP8 Confocal Microscope in bright field mode.

Results and discussion

As outlined in Scheme 1, the 2D microgel CCs were fabricated by *in situ* fixing the first 111 plane of 3D microgel CCs *via* a benzophenone (BP)-based photochemical reaction. The PNIPAM microgels used in the study were prepared by free-radical precipitation polymerization.[27] As reported previously, these microgels all experience a volume phase transition upon heating, as shown in Fig. S1.†[25–27] Unless otherwise specified, the 1450 nm microgel was used in the following studies.

Quartz slides were used as substrate to fabricate the 2D CCs. To introduce the photosensitizer, BP, onto the surface, the slides were first treated with a silane coupling agent with a carboxylic acid end functional group to introduce carboxylic acid groups. The carboxylic acid groups were then activated with EDC/NHS and coupled with 4-aminobenzophenone (ABP)[41] (Scheme 2). The amount of carboxylic acid groups on quartz slide surface was determined by a colorimetric method based
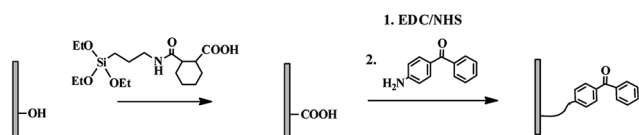
on Toluidine Blue O staining,[41] which is 8.78×10^{-8} and 1.11×10^{-8} mol before and after ABP coupling (Fig. S2†). The result indicated that ∼87% carboxylic acid groups reacted with ABP.

Subsequently, 3D microgel CC was assembled on the functionalized quartz slides. For this purpose, the microgel dispersion was concentrated by centrifugation and then loaded in a cell composed of two quartz slides, one of which was functionalized with BP. As reported previously, the monodisperse microgel particles gradually self-assembled into highly ordered crystalline structure.[46–49] As a result, the samples exhibit iridescent colors when illuminated with white light obliquely (Fig. 1A).[50] The 3D assembly was examined with an optical microscope to investigate its crystal structure, as the microgel spheres are large enough to be visualized with an optical microscope. Fig. 1B shows a representative image, which indicates that the microgel spheres are arranged into a hexagonally close-packed crystalline array. The fast Fourier transformation (FFT) of the image shown in the inset confirms a structure with long-range order and hexagonal symmetry.[51] In the image, the microgel spheres appear to be in intimate contact with one another. The average center-to-center distance between two adjacent particles was determined to be ∼1000 nm, which is smaller than the hydrodynamic diameter (D_h) of the microgel measured as free particles in solution. The different size of the microgel particles in the 3D assembly and solution suggests that the particles experienced a compression during centrifugation and crystallization.[52]

It is noteworthy that the image shown in Fig. 1B was taken from the interior part of the assembly. For the fabrication of 2D CC, the key is that the microgel particles close to the substrate should also self-assemble into ordered structure. Therefore the structure of the first layer of microgel particles close to substrate
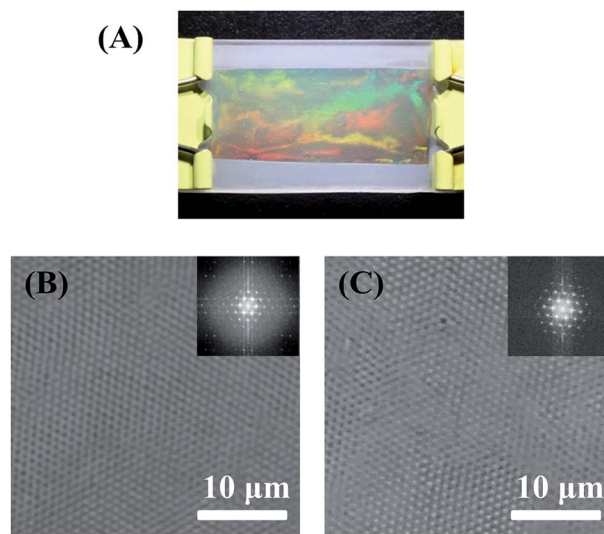
Fig. 1 3D colloidal crystal assembled from the 1450 nm microgel. (A) Photograph of a sample obliquely illuminated with white light. (B) Optical micrograph of the interior region of the 3D colloidal crystal. The inset shows the FFT of the image. (C) Optical micrograph of the layer close to the substrate. The inset shows the FFT of the image (scale bars: 10 μm).

Scheme 2 Introduction of BP groups onto the surface of quartz slide.
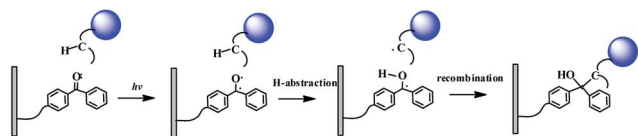
Scheme 3 Attachment of PNIPAM microgel particles onto quartz slide *via* photochemical reaction between BP chromophore and microgel particles.

Fig. 2 AFM (A–C) and optical microscopy images (D–F) of 2D CCs from 1450 nm microgel. Concentration of the microgel dispersion is 3.62 wt% (A and D), 2.85 wt% (B and E), 2.32 wt% (C and F), respectively. The interparticle distance is ~1000 nm (A and D), ~1170 nm (B and E), and ~1300 nm (C and F), respectively. Scale bar: 2 μm.

Fig. 3 AFM images of 2D microgel arrays (A) using un-modified quartz slide as substrate, and (B) using BP-modified slide as substrate but without UV irradiation. Scan bar: 2 μm.

was studied. The image and the corresponding FFT shown in Fig. 1C reveals that these particles also form a highly ordered array, just like the particles in the interior region. Previously Lyon *et al.*[52] also observed that microgel particles assemble into ordered structure along the container wall, which actually form the first 111 plane of the face-centered cubic (fcc) lattice of the 3D CC. The 111 planes in the internal region of the 3D crystal are all parallel to the substrate.[51,52] Compared to the interior region, the degree of order close to the substrate is not reduced, suggesting the existence of the substrate have little influence on the assembly of the microgel particles. Previously Alsayed *et al.*[53] even found that the container wall may stabilize the crystal and therefore the region close to the wall has less defects.

In order to fix the first layer of microgel particles onto the substrate, the crystallized sample was illuminated with UV light (Scheme 1). According to previous studies,[39] when exposed to UV light, the BP chromophores on the substrate will absorb a photon at ~350 nm, which will promote one electron from a nonbonding sp^2-like n-orbital on oxygen to an antibonding π*-orbital of the carbonyl group (Scheme 3). The resulting triplet is biradical in nature which is ready to react with groups in its vicinity. Particularly the oxygen of the carbonyl group will abstract a hydrogen atom from the polymer chain of PNIPAM microgel particle, leaving behind two radicals, one at the previous carbonyl carbon and the other on the polymer chain. The two radicals will eventually recombine, leading to the covalent attachment of the microgel particles to the surface.

Fig. 2 shows the AFM and optical microscopy images of the resulting 2D arrays. Representative large area microscopy images were shown in Fig. S3 in the ESI.† As expected, arrays with highly ordered structure were obtained. The results suggest that the ordered structure of the microgel array close to the substrate was remained because the microgel particles were fixed onto the substrate *in situ*. In addition, because the particles were fixed *via* covalent bonds, the following washing in water and drying in the air do not disturb the pre-formed ordered structure.

To ensure that the successful fabrication of the ordered arrays is indeed due to the light-induced coupling of the surface BP groups to the polymer chains of the microgel particles, two control experiments were designed. In the first control, unmodified quartz slides were used instead of BP-modified ones. Similarly the samples were UV-irradiated followed by a washing procedure. As shown in Fig. 3A, some microgel particles were missing, suggesting they were washed away because of the relatively weak interaction between the particle and the substrate. In addition, the particles were not arranged
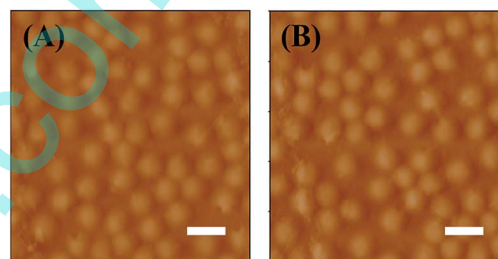
in an ordered structure. In the second control, a BP-modified slide was used, but the UV irradiation step is omitted. Again some particles were found missing and the resulting array is unordered (Fig. 3B). These results indicate that BP modification of the substrate and UV irradiation are essential for the attachment of the microgel particles and maintaining the ordered structure. Previously the same photochemical reaction was exploited to attach various polymers onto BP-modified surfaces.[40,41] It is noteworthy that the BP-based photochemical attachment was usually carried out in dry state.[40,41] In the present case, however, the reaction undergoes in the presence of solvent (water). Despite of this, the images shown in Fig. 2 indicate that the microgel particles could still be effectively attached on the substrate. It was previously found that BPs react preferentially with unreactive C–H bonds, even in the presence of solvent water and bulk nucleophiles.[39]

In order to characterize the ordering of the 2D arrays quantitatively, the dimensionless pair correlation function, $g(r)$, was calculated. $g(r)$ is defined by the following equation:

$$g(r) = \frac{1}{\langle \rho \rangle} \frac{\mathrm{d}n(r, r + \mathrm{d}r)}{\mathrm{d}a(r, r + \mathrm{d}r)} \quad (1)$$
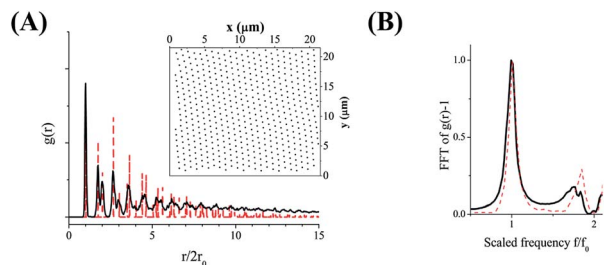
Fig. 4 (A) Pair correlation function, $g(r)$, of the 2D CC from 1450 nm microgel. Dash vertical lines indicate the peaks of $g(r)$ of an ideal hexagonally packed monolayer generated numerically. The inset highlights the centers of the particles as found from the automated particle location procedure. (B) Single-sided power spectra Fourier transforms (FT) of $g(r)$ compared to FT of the corresponding perfectly ordered arrays. The power spectra were scaled to have identical maxima at $f/f_0 = 1.0$.[6]

Fig. 5 Diffraction pattern of normally incident laser beam transmitted through a 2D microgel CC.

where $\langle \rho \rangle$ is the average particle number density, a the shell area and $n(r, r + dr)$ the number of particles that lie within the shell considered.[6,54] To calculate the function, the particle coordinates in the images were determined using ImageJ with the Analyze Particles plugin.[23] Because the function $g(r)$ describes the probability of finding a particle at a distance r from a given particle in the 2D space, the peaks in the distribution indicate the preferred distances and are considered as a signature of order of the 2D array. Fig. 4A shows a typical $g(r)$ of a 2D microgel CC. The inset shows the centers of the particles in the array. For comparison, $g(r)$ of a perfectly packed hexagonal array was also plotted. One can see $g(r)$ of the 2D array displays a series of peaks, suggesting the extension of structural order over a long distance. In addition, the positions of the peaks coincide with those of the perfectly packed hexagonal array, confirming hexagonal packing of the particles.

From $g(r)$, another quantitative measure of ordering, i.e., the ratio of the full width at half maximum of the first peak in the Fourier transform of the function $g(r) - 1$, k, to that of a perfectly packed array, k_0, can be extracted.[6,54] As shown in Fig. 4B, the k/k_0 value was determined to be 1.08. It is known that the ratio is 1 for an array with a perfectly packed structure, and it becomes larger with increasing disorder in the structure. Particularly a k/k_0 less than 1.5 indicates a highly ordered structure, while a k/k_0 larger than 1.5 indicates significant disordering.[6,54] Here the k/k_0 value is close to 1, suggesting the 2D microgel array is highly ordered.

The structure of the microgel arrays was also studied by laser diffraction, a convenient method to examine if the particles in a 2D array are arranged into ordered structure.[50,55] If the particles form a perfect hexagonal crystal, when illuminated with monochromatic laser light, a diffraction pattern composed of a set of distinct spots with 6-fold symmetry will be obtained.[55] As expected, the microgel CC displays a diffraction pattern with six symmetrical spots, confirming again its highly ordered structure (Fig. 5). Many previously reported 2D CCs display a diffraction pattern of a sharp circle (Debye ring), instead of distinct spots. The reason lies that the samples are composed of crystallites with a size significantly smaller than the beam
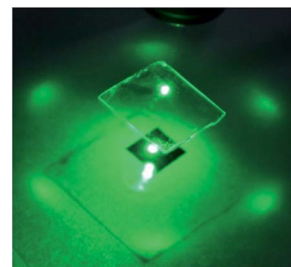
diameter and the crystallites are randomly oriented.[50,55] Here the 2D microgel CC displays a diffraction pattern with symmetrical distinct spots, suggesting that the microgel particles in the illuminated area ($\sim$2 mm in diameter) are arranged perfectly into a hexagonal crystalline array.

Recently Bagheri et al. used a set of parameters to assess the ordering in colloidal crystals.[56] Some of the parameters were also calculated for the 2D microgel CC (Table 2). Lindemann parameter, α, defined as the standard deviation of the distribution of displacements divided by the ideal lattice spacing, is a measure of the local positional disorder.[57] This parameter was found to fall in a narrow range from 0.03 to 0.10 for CCs reported previously.[56] For the 2D CC of the 1450 nm microgel, the parameter was calculated to be 0.042,[58,59] falling in the same range for other CCs. Local bond orientational order for 6 fold symmetry, defined as

$$\Psi_6 = \left| \frac{1}{N} \sum_{j=1}^{N} e^{i6\theta_j} \right| \quad (2)$$

where N is the number of the nearest neighbours at the lattice point, and θ_j is the angle between a reference axis and the line connecting that lattice point to its jth nearest neighbour, is considered the best indicator of local order for real crystals.[56] For perfectly packed hexagonal array the value is 1. A Ψ_6 value of 0.981 was determined for the 2D CC of the 1450 nm microgel, closing to that of a perfectly packed array. The CCs reported previously also have a Ψ_6 value close to 1.[56] As for long range order parameter, the positional correlation length ξ_6, was also extracted from pair correlation function $g(r)$ according to Bagheri et al.[56] A ξ_6 value of 3.16 was determined for the 2D CC of the 1450 nm microgel. According to Bagheri et al.,[56] most of the CCs reported previously have a ξ_6 value between 2 to 6. Some CCs with an extraordinary high ξ_6 value were also reported.

Besides the 1450 nm microgel, three other microgels, with size varying from 880 nm to 1800 nm, were also used to fabricate 2D arrays. The AFM and optical microscopy images of the resulting arrays were shown in Fig. 6. As the images indicated, all these microgels were arranged into a hexagonal crystalline array. Again the average center-to-center distance between two adjacent particles was found to be smaller than D_h of the microgel as free particles in solution. For example, the array shown in Fig. 6A and D was fabricated from microgel with a D_h of 880 nm, while the average interparticle distance of the array

Table 2 Lindemann parameter (α), local orientational bond order (Ψ_6) and positional correlation length (ξ_6) of the 2D microgel CCs

2D microgel CCs	Image size (μm^2)	α	Ψ_6	ξ_6
880 nm microgel	12×12	0.061 ($\pm$0.003)	0.92 ($\pm$0.02)	2.08 ($\pm$0.07)
1450 nm microgel	40×40	0.042 ($\pm$0.001)	0.98 ($\pm$0.01)	3.16 ($\pm$0.03)
1550 nm microgel	30×30	0.051 ($\pm$0.002)	0.95 ($\pm$0.02)	2.90 ($\pm$0.06)
1800 nm microgel	20×20	0.050 ($\pm$0.002)	0.96 ($\pm$0.01)	3.88 ($\pm$0.09)
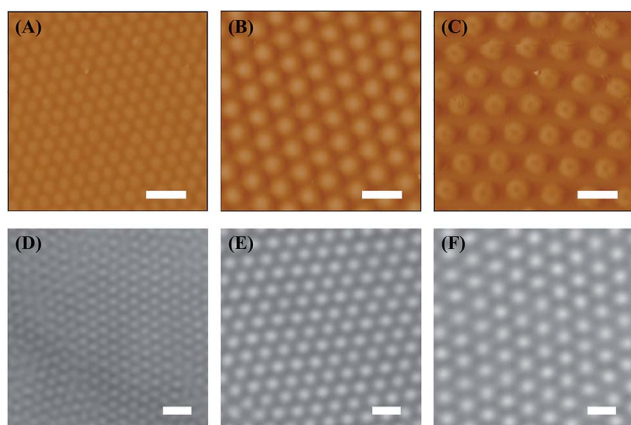
Fig. 6 AFM (A–C) and optical microscopy images (D–F) of the 2D arrays fabricated from microgels of different sizes. The microgel particle size is 880 nm (A and D), 1550 nm (B and E), and 1800 nm (C and F), respectively. Scale bar: 2 μm.

was ∼800 nm. The pair correlation function, $g(r)$, of the 3 arrays was also calculated and shown in Fig. S4.† k/k_0 value was determined to be 1.02, 1.38, and 1.48 for 2D array fabricated from 880 nm, 1550 nm, and 1800 nm microgel, respectively (Fig. S5†). These results confirm again a highly ordered structure of these arrays. Meanwhile, Lindemann parameter, α, local orientational bond order, Ψ_6, and positional correlation length, ξ_6, of the 2D microgel CCs were also calculated (Table 2). These values are comparable to the corresponding one of the CC from 1450 nm microgel.

To study the effect of the concentration of the dispersion, 2D arrays were fabricated using different concentration of 1450 nm microgel. As shown in Fig. 3, the interparticle distance of the 2D arrays decreases with increasing dispersion concentration. For the 2D array from 2.32 wt% dispersion, the interparticle distance is ∼1300 nm. This value reduces to be ∼1000 nm when the concentration increases to 3.62 wt%. From Scheme 1, the interparticle distance of the 2D array is determined by the interparticle distance of the 3D CC. It was previously revealed that the lattice constant of a 3D microgel CC can be tuned by varying the concentration of the microgel dispersion.[46,47] In a higher concentration dispersion, the microgel particles will be compressed to a larger degree. Crystallization of the dispersion results in a 3D crystal with a reduced interparticle distance and hence a shorter lattice constant.[46,47] Accordingly when the first 111 plane of the 3D CC is fixed *in situ* on the substrate, a 2D array with a shorter interparticle distance will be obtained.

It is highly desirable that a method can fabricate large scale 2D CCs. Unfortunately, most of the existing methods can only produce arrays with a relatively small size. Previously Asher *et al.*[6] developed a method to assemble large area 2D arrays from hard colloids. An advantage of the method developed here is that it allows to produce 2D microgel CCs with any size, because 3D microgel CCs of any size can be facilely fabricated.[37] In the above work we used quartz slides with a size of 4.5 cm × 2.5 cm as substrate. The area of the resulting 2D CC is ∼7.5 cm². To demonstrate the ability to fabricate large size 2D CCs, a quartz slide with a size of 11 cm × 11 cm was used. The resulting 2D CC has an area of ∼61 cm². When illuminated with white light obliquely from behind, the 2D CC displays vivid diffraction color (Fig. 7A), suggesting a highly ordered structure. Like other 2D CCs reported previously, different parts of the array display different colors, which can be explained by the different angle at which the individual part is illuminated.[6,50] The polycrystalline nature of the array[46] may be a second reason for the observed different colors.

Most of the methods for 2D CC fabrication can only use planar substrates. In contrast, the method developed here allows for the fabrication of 2D CC on nonplanar substrates. As an example, the inner wall of a test tube with an inner diameter of 0.8 cm was modified with BP chromophore. Concentrated microgel dispersion was then added. After the dispersion crystallized, the tube was UV-irradiated. As shown in Fig. 7B, the tube also displays vivid diffraction color when illuminated with white light obliquely from behind. The result suggests that a crystalline array of microgel particles was successfully fabricated on the inner surface of the tube.
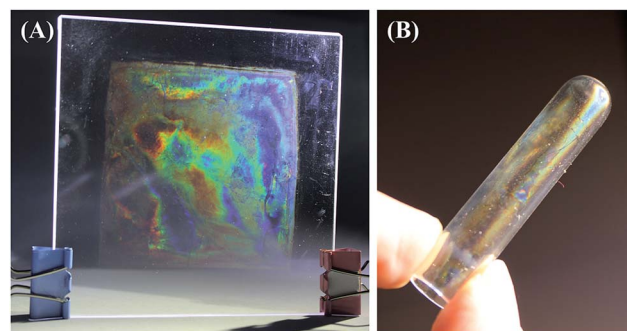
Fig. 7 (A) Photograph of a 2D microgel CC fabricated using an 11 cm × 11 cm quartz slide as substrate. (B) A 2D microgel CC fabricated on the inner wall of a test tube.

Conclusions

In conclusion, we fabricated 2D microgel CCs by first assembling the microgel spheres into a highly ordered 3D CC, followed by fixing the first 111 plane of the 3D CC onto the substrate *via* a BP-based photochemical reaction. In the 3D microgel CC, like ones in the interior region, the particles close to the substrate were also arranged into highly ordered structure. Under UV irradiation, covalent bonds forms between the BP groups on the substrate surface and the polymer chains of the microgel particles. As a result, the microgel particles close to the substrate were covalently bound onto the substrate. As they were fixed *in situ*, their highly ordered structure was maintained. Because large size 3D microgel CC can be facilely synthesized, this method allows for fabrication of large area 2D microgel CC. Beside planar substrate, 2D microgel CCs can also be fabricated on nonplanar substrates. In addition, the interparticle distance in the 2D CCs can be tuned by the concentration of the microgel dispersion. Because the BP-based photochemical reaction was chosen for the fixing purpose, instead of the photo-initiated thiol–ene reaction as we used before,[38] the modification of the microgel particles is no longer needed.

Acknowledgements

Notes and references

1 Y. N. Xia, B. Gates, Y. D. Yin and Y. Lu, *Adv. Mater.*, 2000, **12**, 693–713.
2 H. Cong, B. Yu, J. Tang, Z. Li and X. Liu, *Chem. Soc. Rev.*, 2013, **42**, 7774–7800.
3 J. Zhang, Y. Li, X. Zhang and B. Yang, *Adv. Mater.*, 2010, **22**, 4249–4269.
4 J. H. Holtz and S. A. Asher, *Nature*, 1997, **389**, 829–832.
5 S. Yang and Y. Lei, *Nanoscale*, 2011, **3**, 2768–2782.
6 J. Zhang, L. Wang, D. N. Lamont, S. S. Velankar and S. A. Asher, *Angew. Chem., Int. Ed.*, 2012, **51**, 6117–6120.
7 J. Zhang, L. Wang, J. Luo, A. Tikhonov, N. Kornienko and S. A. Asher, *J. Am. Chem. Soc.*, 2011, **133**, 9152–9155.
8 D. Men, H. Zhang, L. Hang, D. Liu, X. Li, W. Cai, Q. Xiong and Y. Li, *J. Mater. Chem. C*, 2015, **3**, 3659–3665.
9 F. Xue, Z. Meng, F. Wang, Q. Wang, M. Xue and Z. Xu, *J. Mater. Chem. A*, 2014, **2**, 9559–9565.
10 N. Vogel, C. K. Weiss and K. Landfester, *Soft Matter*, 2012, **8**, 4044–4061.
11 S. B. Quint and C. Pacholski, *Soft Matter*, 2011, **7**, 3735–3738.
12 P. Jiang, T. Prasad, M. J. McFarland and V. L. Colvin, *Appl. Phys. Lett.*, 2006, **89**, 11908.
13 P. Jiang and M. J. McFarland, *J. Am. Chem. Soc.*, 2004, **126**, 13778–13786.

14 P. Jiang and M. J. McFarland, *J. Am. Chem. Soc.*, 2005, **127**, 3710–3711.
15 X. Ye and L. Qi, *Sci. China: Chem.*, 2014, **57**, 58–69.
16 P. Born, A. Munoz, C. Cavelius and T. Kraus, *Langmuir*, 2012, **28**, 8300–8308.
17 M. Kargar, A. Pruden and W. A. Ducker, *J. Mater. Chem. B*, 2014, **2**, 5962–5971.
18 R. Ye, Y. Ye, Z. Zhou and H. Xu, *Langmuir*, 2013, **29**, 1796–1801.
19 X. Sun, Y. Li, T. H. Zhang, Y. Ma and Z. Zhang, *Langmuir*, 2013, **29**, 7216–7220.
20 E. C. H. Ng, K. M. Chin and C. C. Wong, *Langmuir*, 2011, **27**, 2244–2249.
21 F. Xue, S. A. Asher, Z. Meng, F. Wang, W. Lu, M. Xue and F. Qi, *RSC Adv.*, 2015, **5**, 18939–18944.
22 F. Xue, Z. Meng, F. Qi, M. Xue and L. Qiu, *Colloid Polym. Sci.*, 2016, **294**, 479–482.
23 H. Yang, N. Gozubenli, Y. Fang and P. Jiang, *Langmuir*, 2013, **29**, 7674–7681.
24 Y. Xia, X. He, M. Cao, X. Wang, Y. Sun, H. He, H. Xu and J. R. Lu, *Biomacromolecules*, 2014, **15**, 4021–4031.
25 J. Y. A. K. Peter, *Rep. Prog. Phys.*, 2014, **77**, 56601.
26 Y. Guan and Y. Zhang, *Soft Matter*, 2011, **7**, 6375–6384.
27 R. H. Pelton and P. Chibante, *Colloids Surf.*, 1986, **20**, 247–256.
28 G. Zhang, D. Wang, Z. Gu, J. Hartmann and H. Möhwald, *Chem. Mater.*, 2005, **17**, 5268–5274.
29 S. Schmidt, T. Hellweg and R. von Klitzing, *Langmuir*, 2008, **24**, 12595–12602.
30 S. Tsuji and H. Kawaguchi, *Langmuir*, 2005, **21**, 8439–8442.
31 Y. Lu and M. Drechsler, *Langmuir*, 2009, **25**, 13100–13105.
32 M. Horecha, V. Senkovskyy, A. Synytska, M. Stamm, A. I. Chervanyov and A. Kiriy, *Soft Matter*, 2010, **6**, 5980–5992.
33 K. Horigome and D. Suzuki, *Langmuir*, 2012, **28**, 12962–12970.
34 K. Geisel, W. Richtering and L. Isa, *Soft Matter*, 2014, **10**, 7968–7976.
35 N. Vogel, C. Fernandez-Lopez, J. Perez-Juste, L. M. Liz-Marzan, K. Landfester and C. K. Weiss, *Langmuir*, 2012, **28**, 8985–8993.
36 A. S. Iyer and L. A. Lyon, *Angew. Chem., Int. Ed.*, 2009, **48**, 4562–4566.
37 T. Hellweg, *Angew. Chem., Int. Ed.*, 2009, **48**, 6777–6778.
38 X. Li, J. Weng, Y. Guan and Y. Zhang, *Langmuir*, 2016, **32**, 3977–3982.
39 G. Dorman and G. D. Prestwich, *Biochemistry*, 1994, **33**, 5661–5673.
40 O. Prucker, C. A. Naumann, J. Rühe, W. Knoll and C. W. Frank, *J. Am. Chem. Soc.*, 1999, **121**, 8766–8770.
41 N. Singh, A. W. Bridges, A. J. Garcia and L. A. Lyon, *Biomacromolecules*, 2007, **8**, 3271–3275.
42 M. D. Barker, R. A. Dixon, S. Jones and B. J. Marsh, *Tetrahedron*, 2006, **62**, 11663–11669.
43 B. E. Campbell, M. Tarleton, C. P. Gordon, J. A. Sakoff, J. Gilbert, A. McCluskey and R. B. Gasser, *Bioorg. Med. Chem. Lett.*, 2011, **21**, 3277–3281.

44 S. Sam, L. Touahir, J. Salvador Andresa, P. Allongue, J. N. Chazalviel, A. C. Gouget-Laemmel, C. Henry De Villeneuve, A. Moraillon, F. Ozanam, N. Gabouze and S. Djebbar, *Langmuir*, 2010, **26**, 809–814.

45 B. Gupta, C. Plummer, I. Bisson, P. Frey and J. Hilborn, *Biomaterials*, 2002, **23**, 863–871.

46 J. D. Debord, S. Eustis, S. B. Debord, M. T. Lofye and L. A. Lyon, *Adv. Mater.*, 2002, **14**, 658–662.

47 J. Gao and Z. B. Hu, *Langmuir*, 2002, **18**, 1360–1367.

48 M. Chen, Y. Zhang, S. Jia, L. Zhou, Y. Guan and Y. Zhang, *Angew. Chem., Int. Ed.*, 2015, **54**, 9257–9261.

49 M. Chen, L. Zhou, Y. Guan and Y. Zhang, *Angew. Chem., Int. Ed.*, 2013, **52**, 9961–9965.

50 B. G. Prevo and O. D. Velev, *Langmuir*, 2004, **20**, 2099–2107.

51 J. Brijitta, B. V. R. Tata, R. G. Joshi and T. Kaliyappan, *J. Chem. Phys.*, 2009, **131**, 74904–74908.

52 S. B. Debord and L. A. Lyon, *J. Phys. Chem. B*, 2003, **107**, 2927–2932.

53 A. M. Alsayed, M. F. Islam, J. Zhang, P. J. Collings and A. G. Yodh, *Science*, 2005, **309**, 1207–1210.

54 R. Rengarajan, D. Mittleman, C. Rich and V. Colvin, *Phys. Rev. E: Stat., Nonlinear, Soft Matter Phys.*, 2005, **71**, 16615.

55 J. Zhang, X. Chao, X. Liu and S. A. Asher, *Chem. Commun.*, 2013, **49**, 6337–6339.

56 P. Bagheri, A. M. Almudallal, A. Yethiraj and K. M. Poduska, *Langmuir*, 2015, **31**, 8251–8259.

57 T. Speck, H. Löwen and J. Bialké, *Phys. Rev. Lett.*, 2012, **108**, 168301.

58 Y. Zhou, M. Karplus, K. D. Ball and R. S. Berry, *J. Chem. Phys.*, 2002, **116**, 2323–2329.

59 Z. Wang, A. M. Alsayed, A. G. Yodh and Y. Han, *J. Chem. Phys.*, 2010, **132**, 154501.